

# Interpretation®

## USING SYNTHETIC DATA TRAINED CONVOLUTIONAL NEURAL NETWORK FOR PREDICTING SUB-RESOLUTION THIN LAYERS FROM SEISMIC DATA

Journal:	<i>Interpretation</i>
Manuscript ID	INT-2022-0059.R1
Manuscript Type:	Technical Paper (if no special section applies)
Date Submitted by the Author:	08-Sep-2022
Complete List of Authors:	Qu, Dongfang; University of Copenhagen; Rambøll A/S, Mosegaard, Klaus; University of Copenhagen: the Niels Bohr Institute, Department of Physics Feng, Runhai ; University of Copenhagen, Niels Bohr Institute Nielsen, Lars; University of Copenhagen, Department of Geosciences and Natural Resource Management
Keywords:	seismic, artificial intelligence, geostatistics, layered, reservoir characterization
Subject Areas:	Structural, stratigraphic, and sedimentologic interpretation, Interpretation concepts, algorithms, methods, and tools, Application examples (applying a relatively new technique or concept), Near-surface, ground penetrating radar, environmental, and engineering applications, Outcrop and subsurface modeling

SCHOLARONE™  
Manuscripts

1  
2  
3  
4 USING SYNTHETIC DATA TRAINED CONVOLUTIONAL NEURAL NETWORK FOR  
5  
6 PREDICTING SUB-RESOLUTION THIN LAYERS FROM SEISMIC DATA  
7

8 Dongfang Qu<sup>1,3\*</sup>(qudongfang2012@gmail.com), Klaus Mosegaard<sup>2</sup> (mosegaard@nbi.ku.dk),  
9  
10 Runhai Feng<sup>2</sup> (runhai.feng@gmail.com), Lars Nielsen<sup>1</sup> (ln@ign.ku.dk)  
11  
12

- 13  
14 1. Department of Geosciences and Natural Resource Management, University of Copenhagen,  
15  
16 Øster Voldgade 10, 1350 Copenhagen, Denmark  
17  
18 2. Niels Bohr institute, University of Copenhagen, 2200 Copenhagen, Denmark  
19  
20  
21 3. Ramboll Danmark A/S, Hannemanns Allé 53, 2300 Copenhagen, Denmark  
22

23  
24 \*Corresponding author  
25

26 Running head:  
27

28  
29 SYNTHETIC DATA-TRAINED DEEP LEARNING FOR SEISMIC INTERPRETATION  
30  
31  
32  
33  
34  
35  
36  
37  
38  
39  
40  
41  
42  
43  
44  
45  
46  
47  
48  
49  
50  
51  
52  
53  
54  
55  
56  
57  
58  
59  
60

Original paper date of submission: 19-05-2022

## ABSTRACT

Numerous studies have demonstrated the capability of supervised deep learning techniques for predicting geological features of interest from seismic sections, including features that are difficult to identify using traditional interpretation methods. However, successful application of these techniques in practice has been limited by the difficulty of obtaining large training dataset where seismic data and corresponding ground truth labels are well defined. Manually creating large amounts of labels requires a heavy workload, and the uncertainty of the interpretation and labeling process decreases the model's ability for making accurate predictions. Using the chalk-flint sequence scenario onshore Denmark as an example, we present a novel workflow of generating large quantities of synthetic training data with high-quality labels using stochastic geological modelling, and we investigate the capability of a synthetic data-trained convolutional neural network for predicting sub-resolution thin layers from seismic sections. It is shown that a neural network trained on synthetic data can predict a realistic number of sub-resolution flint layers from real seismic data that have been collected from the Stevns region in Denmark, which has value for understanding of overall geological characteristics of the succession and engineering applications such as construction site evaluation.

## INTRODUCTION

1  
2  
3  
4  
5  
6 With the increasing availability of computing powers, supervised deep learning techniques,  
7 particularly the end-to-end convolutional neural network (e.g. U-net), have been increasingly used  
8 for predicting geological features of interest from seismic data (Li et al., 2019; Wu et al., 2019;  
9 Feng et al., 2021). They have shown advantages in not only higher efficiency but also capability  
10 for predicting features that are normally difficult to identify as compared to traditional  
11 interpretation methods (Dramsche, 2020). A critical factor for achieving success using this approach  
12 is the availability of large amounts of training data where seismic data and corresponding ground  
13 truth labels are well defined (Merrifield et al., 2022). This is difficult as data in geoscience is often  
14 expensive, sparse, uncertain and biased, some are not even machine-readable (Dramsche, 2020).  
15 Creating large amounts of labels requires firstly interpreting the geological features of interest  
16 from seismic data, and then manual labelling, which may not be feasible in practice. Moreover,  
17 the uncertainties related to such an interpretation and labeling process can decrease the model's  
18 ability for making accurate predictions.  
19  
20  
21  
22  
23  
24  
25  
26  
27  
28  
29  
30  
31  
32  
33  
34  
35

36 One way of generating large quantities of training data with high quality labels is to create  
37 synthetic data (Merrifield et al., 2022). Several deep learning projects used synthetically generated  
38 seismic data including computer-generated labels for predicting geological features from seismic  
39 data sections and produced promising results (e.g. Wu et al., 2019; Merrifield et al., 2022). These  
40 existing studies are mainly focused on large-scale features that can be easily identified by the  
41 human eye, such as large-scale faults, salt domes, and layers with thicknesses larger than the  
42 seismic resolutions. Prediction of thin layers that are below the resolution of seismic data has not  
43 been studied. In this paper, we show the capability of synthetic data-trained deep neural network  
44 for predicting sub-resolution thin layers from seismic data.  
45  
46  
47  
48  
49  
50  
51  
52  
53  
54  
55  
56  
57  
58  
59  
60

## SEISMIC INTERPRETATION CHALLENGES

Mapping the distribution of individual layers of specific lithology or soil type from seismic data is demanded in many geoscience applications, including characterization of near-surface materials at planned construction site, characterization of hydrocarbon and groundwater reservoirs, etc. Yet it is a challenging task as the layers of interest can be too thin to be resolved by the seismic data. Seismic interpretation provides only formation boundaries, not boundaries between sub-resolution layers. Seismic inversion could potentially resolve rock physical properties from which the layer boundaries can be interpreted, but the inversion resolution is limited by e.g. the intrinsic tuning effects, incomplete knowledge of the seismic wavelet and noise in the data (Phan, 2021). Geostatistical seismic inversion makes use of statistical information and could potentially provide a higher inversion resolution, but it relies on a geostatistical simulation algorithm generating multiple realistic geological realizations, which becomes difficult when the geometry and spatial arrangement of the layers are too complex to be simulated in an efficient way (Wang et al., 2022).

For example, the chalk and flint layers widely distributed in onshore SE Denmark have contrasting physical and geotechnical properties. Mapping their spatial distribution is needed for e.g. characterization of construction sites and groundwater resource planning, but is also challenging as the abundant and important flint layers are so thin (ca. 20 – 30 cm) that reflected signals from closely spaced layer boundaries interfere with each other and generate misleading composite signals (Qu et al., 2022). Bedding architectures are furthermore variable due to a dynamic depositional environment in which the sediment was formed; horizontal bedding, wavy bedding, onlap, downlap, and pinch-out can coexist in the same sequence and only hand-drawing can reproduce the bedding architectures in full detail (Anderskov et al., 2007, Qu et al., 2022).

1  
2  
3 Thus, some questions that are interesting to be investigated are as follows: Is it possible to  
4 predict the correct number of thin layers from seismic sections where the reflected signals are  
5 highly interfering with each other? Can a neural network trained on synthetic examples with  
6 simple and regular layering architectures manage to predict more complex and variable layering  
7 architectures? Can a neural network trained on synthetic seismic data make predictions on real  
8 seismic data?  
9  
10  
11  
12  
13  
14  
15  
16

17 In this study, we use the chalk-flint sequence scenario in onshore Denmark as an example,  
18 to develop and present a workflow of generating large quantities of relevant and diverse synthetic  
19 training data. We firstly generate the synthetic examples using stochastic geological modelling and  
20 seismic forward modelling. Then we train a convolutional neural network based on the synthetic  
21 training data, and we test the performance of the trained neural network on both new synthetic  
22 seismic data and real seismic data that have been acquired from the Stevns region in Denmark. In  
23 this paper, thin layers are defined as ones whose thickness is below the resolution of seismic data,  
24 i.e. one fourth of the wavelength, which is below 3 – 4 m with the dominant frequency of 150 Hz.  
25 In our study, all flint layers in the chalk-flint sequence scenario considered are around 20 – 30 cm  
26 thick, and thus are sub-resolution thin layers.  
27  
28  
29  
30  
31  
32  
33  
34  
35  
36  
37  
38  
39  
40

#### 41 SYNTHETIC TRAINING DATASET

42  
43 One way to create relevant synthetic examples is to make the most of available information,  
44 e.g. previous geological studies about the formation of interest, lithology types revealed by  
45 borehole data, outcropping sections of the same formations or other formations deposited in similar  
46 environments. In this study, prior knowledge of the geometry and physical properties of the layers  
47 in the chalk-flint sequence in onshore Denmark has been taken into consideration for creating the  
48  
49  
50  
51  
52  
53  
54  
55  
56  
57  
58  
59  
60

1  
2  
3 synthetic examples (e.g. Surlyk et al., 2006; Anderskouv et al., 2007; Nielsen et al., 2011;  
4  
5 Kammann et al., 2019; Yuan et al., 2021).  
6  
7

## 8 **Geological models**

9

10  
11 After obtaining an understanding of the lithology types occurring in the formation of  
12  
13 interest and possible thickness and spatial distributions from prior knowledge, we develop a  
14  
15 modeling method that can honor the known information. It is important that large amounts of  
16  
17 geological models can be generated in an automated, efficient manner without heavy manual work,  
18  
19 otherwise the advantage of the synthetic data-trained deep learning approach would be reduced.  
20  
21 Our strategy is to make relevant geological models based on known geological information, but  
22  
23 ignore some complex bedding architecture features. We will then test the generalization ability of  
24  
25 the deep learning model to investigate if it can predict the complex bedding phenomena not  
26  
27 included the training examples.  
28  
29  
30  
31

32 The sequence of interest in this study consists of interbedded chalk and flint layers, in  
33  
34 which the thickness of chalk layers varies laterally, while the thickness of flint layers is assumed  
35  
36 constant. We generate various interbedded chalk-flint sections using a published carbonate mound  
37  
38 modelling strategy (Janson and Madriz, 2012). The thickness of each chalk layer bounded between  
39  
40 two flint layers is modelled using a variogram-based stochastic geostatistical modelling method,  
41  
42 i.e., sequential Gaussian simulation (SGS). A flint layer with constant thickness is added on top of  
43  
44 each chalk layer. The chalk layer thickness and variogram range of the thickness variation in the  
45  
46 lateral direction are chosen randomly with some constraints, which are based on prior knowledge  
47  
48 of the geometry of the well-known chalk strata (e.g. Surlyk et al., 2006; Anderskouv et al., 2007).  
49  
50  
51 In the case when little information is available about the input parameters, a wide constraining  
52  
53  
54  
55  
56  
57  
58  
59  
60

1  
2  
3 range can be applied for each input parameter to capture different possibilities resulting from the  
4  
5 uncertainty.  
6  
7

8           500 geological sections with different numbers of layers and varying geometries are  
9  
10 generated, constrained by a mean chalk layer thickness between 1 and 10 meters and a variogram  
11  
12 range of the thickness variation between 20 and 500 meters. Each section has  $256 \times 2560$  pixels,  
13  
14 with each pixel representing 0.1 m in space and 0.07 ms in time (Figure 1). Each flint layer has a  
15  
16 constant thickness of three pixels. The chosen resolution is decided by considering the thin  
17  
18 thickness of the high-velocity flint layers and the numbers of flint layers to be included in the  
19  
20 sections. We would like to have enough pixels to represent the thin and wavy flint layers, but also  
21  
22 would like to have the possibility of including more flint layers in the sections such that the  
23  
24 interference effect contributed by different numbers of interfaces can be captured.  
25  
26  
27

28  
29           Two sections of interbedded strata with different numbers of layers and different layer  
30  
31 geometries are shown in Figures 1a and b. It needs to be noted that some complex phenomena  
32  
33 observed from outcropping sections, such as wedge-shaped onlap, are not included in the synthetic  
34  
35 examples. It would be a huge advantage of this approach if the model trained on examples with  
36  
37 simple bedding phenomena can predict complex bedding phenomena. We will train a model using  
38  
39 this dataset including only simple bedding phenomena and apply it on cases exhibiting complex  
40  
41 phenomena not present in the training dataset. Thus the generalization ability of the deep learning  
42  
43 model on unseen data with unseen geological features can be tested.  
44  
45  
46

### 47 48 **Seismic synthetics** 49

50  
51           The geological sections are transformed to acoustic impedance sections by assigning  
52  
53 realistic P-wave velocity and bulk density values for flint layers and chalk layers, such as 5500  
54  
55 m/s and  $2800 \text{ kg/m}^3$  for flint, and 2300 m/s and  $2700 \text{ kg/m}^3$  for chalk (Qu et al., 2022). Reflectivity  
56  
57

1  
2  
3 sections are then computed. The seismic images are generated by performing a 2D convolution of  
4 the reflectivity matrix and a 2D Ricker wavelet matrix, and returning the central part of the  
5 convolution that has the same size as the reflectivity matrix (Figure 1c, d). A 10% white Gaussian  
6 noise is added to each seismic image.  
7  
8  
9  
10

11  
12  
13 Considering the fact that any practical migration will result in a somewhat smoothed  
14 response laterally, we use a 2D wavelet with a ‘hyperbolic’ shape and decreasing amplitude away  
15 from the center to simulate an imperfectly migrated response from a point scatterer. The horizontal  
16 width and bending of the wavelet take account of the remaining horizontal smearing after data  
17 migration, and are adjustable. A wider wavelet produces more horizontal smearing; a more bended  
18 wavelet generates synthetics mimicking under-migrated or over-migrated seismic data. In this  
19 paper, these parameters are adjusted based on one of our test examples, such that the synthetics  
20 generated using this method can be similar to the seismic image used as a test. The dominant  
21 frequency of the Ricker wavelet used in this paper is 150 Hz (Figure 2), consistent with the  
22 dominant frequency of our seismic data on which the trained neural network is to be applied.  
23  
24  
25  
26  
27  
28  
29  
30  
31  
32  
33  
34  
35

36 These 500 pairs of geological sections and corresponding seismic images are then split into  
37 5000 pairs of smaller patches, each has a resolution of  $256 \times 256$  pixels (Figure 3). The amplitude  
38 of each big seismic image is scaled to a range between -1 and 1 prior to splitting.  
39  
40  
41  
42  
43  
44  
45  
46

## 47 NETWORK TRAINING

### 48 **Network architecture**

49  
50  
51 For each pixel in the seismic image, we would like to know the category it belongs to (flint  
52 layer or not), which is a binary segmentation problem. We use a U-net architecture to perform this  
53  
54  
55  
56  
57

segmentation task. U-net was originally developed for biomedical image segmentation (Ronneberger et al., 2015), and it has later on been successfully used for seismic interpretation (Li et al., 2019; Wu et al., 2019). It has an important advantage in requiring less training images and yielding more precise segmentations (Ronneberger et al., 2015).

The U-net that we use for thin layer segmentation consists of a contracting path and a symmetric expanding path that enables precise localization (Figure 4). The left contracting path consists of four convolution groups and each group is followed by a  $2 \times 2$  max pooling to halve the image size. Each convolution group involves two  $3 \times 3$  convolutions, each followed by a ReLU activation (Nair and Hinton 2010) and a batch normalization (Ioffe and Szegedy 2015). In each convolution operation, a feature detector, also known as a kernel or a filter, moves across the layer's input matrix and generates a feature map; the value of each pixel in the feature map is a dot product of the filter with the area of the input matrix around that pixel. A set of learnable filters are applied in each convolution layer, and multiple feature maps are generated. In the contracting path, the image size decreases as the number of channels increases, and the image size reaches a minimum at the bottom. In the right expanding path, every step consists of an operation that doubles the image size and halves the number of feature channels, a concatenation with the corresponding feature image from the contracting path, and two convolutions, each followed by a ReLU activation and a batch normalization. Finally, the output size is restored to that of the original image, which is  $256 \times 256$  in this case. At the end of the network, a  $1 \times 1$  convolution followed by a Sigmoid function (equation 1) outputs the probability of each pixel belonging to category 1 (i.e. the flint layer).

$$S(x) = \frac{1}{1 + e^{-x}} \quad (1)$$

## Loss function

Commonly used loss functions such as binary cross-entropy require a more or less balanced distribution of zeros and non-zeros (Wu et al., 2019; van Beers et al., 2019), which is not the case here, as the geological scenarios are dominated by the chalk background.

In this paper, we use a loss function based on the Jaccard Similarity Coefficient, also known as intersection-over-union (IoU). IoU measures the similarity between the predicted region and the ground-truth region for an object present in the image and is often used as a measure of success. It is defined as the size of the intersection divided by the size of the union of two sets (Rahman and Wang, 2016), and takes into account of the class imbalance issue. The loss function used in this paper is defined in terms of an approximation of the IoU, which becomes differentiable (van Beers et al., 2019). The definition of the metric and loss function used to train the network are written as follows:

$$\text{Metric} = \frac{T * P + 1}{T + P - T * P + 1} \quad (2)$$

$$\text{Loss} = - \frac{T * P + 1}{T + P - T * P + 1} \quad (3)$$

Where T is the True image composed of 1s and 0s, P is the predicted image composed of probability values between 0 and 1, T\*P is the element-wise multiplication of T and P.

## Training

We use 4250 pairs of the geological and seismic patches as training data and the rest 750 pairs as validation data. The Adam method is used to optimize the network parameters (Kingma and Ba, 2014). The batch size is 32. Number of epochs to train the network is set to 70, but with an early stopping option – training will be stopped if the monitored metric has no improvement after 5 epochs. The learning rate will be reduced with a factor of 0.1 when the metric has stopped improving after 3 epochs, with a minimum learning rate of 0.00001.

1  
2  
3 Figure 5 shows that the training and validation loss decrease with the increase of epochs,  
4 and the loss on the validation set stops decreasing after 45 epochs. We run the proposed network  
5  
6  
7  
8 model using NVIDIA Quadro P5000 GPU, and the training takes 20 minutes.  
9

## 10 TEST AND RESULTS

11  
12  
13 We test the performance of the trained neural network on two synthetic examples and one  
14 real example. As the neural network is trained on image patches with size of  $256 \times 256$ , the seismic  
15  
16 images to apply it on are divided into patches of size  $256 \times 256$ , on which the predictions are made.  
17  
18  
19 The predicted geological image patches are reconstructed to form complete images afterwards.  
20  
21  
22

23 The prediction outputs probability of each pixel belonging to the category of flint. The  
24 probability section is then converted to category sections by using a threshold value of 0.5, i.e.  
25  
26 pixels with probability values higher than 0.5 are classified as flint. The prediction results are  
27  
28  
29 visually compared to either ground truth labels (if available) or outcropping geological sections  
30  
31 nearby the seismic data, and they are evaluated in terms of predicted numbers of flint layers,  
32  
33 geometries, and continuity.  
34  
35  
36

### 37 **Test on synthetic example similar to the training data**

38  
39  
40 We first test the performance of the trained neural network on a synthetic example  
41 generated by the same modeling algorithm used for generating the training dataset, but not used in  
42  
43 the training and validation process (Figure 6). The ground truth geological scenario is an  
44  
45 interbedded sequence consisting of 10 flint layers and 11 chalk layers, all below the seismic  
46  
47 resolution (Figure 6b). The strata pattern is similar to that of the training examples; all layers are  
48  
49 continuous. The synthetic seismic image shows three to four discontinuous reflections, due to  
50  
51  
52  
53  
54  
55  
56  
57  
58  
59  
60

1  
2  
3 interference of reflected signals from closely spaced layer boundaries (Figure 6a; Qu et al., 2022).  
4  
5 These sub-resolution layers are difficult to interpret from the seismic image.  
6  
7

8 Figure 6c shows the result predicted by the trained neural network. The number of layers,  
9  
10 the thickness of each layer, and the gently wavy geometry are well predicted. Continuity artifacts  
11  
12 can be observed at some places (e.g. the red circles in Figure 6c), this is because the flint layers  
13  
14 are so thin (only three pixels thick) that any tiny inaccuracy can cause discontinuity. Increasing  
15  
16 the resolution of the image might improve the continuity of the predicted layers.  
17  
18

### 19 20 **Test on synthetic example different from the training data** 21 22

23 It is not surprising that the trained convolutional neural network works well in the first test  
24  
25 as the test data are drawn from the same statistics as the ones used for the training data – all have  
26  
27 simple strata patterns. The real strata patterns of the onshore chalk succession in SE Denmark are  
28  
29 more complex; some units can contain onlap and downlap phenomena, which are not included in  
30  
31 the training dataset. Would the convolutional neural network trained on examples with simple  
32  
33 bedding architectures be able to extrapolate and predict more complex bedding architectures?  
34  
35

36  
37 In the second test, we apply the trained model on a seismic section whose ground truth  
38  
39 label contains new bedding features such as onlap, downlap and pinch-out (Figure 7b). Interference  
40  
41 of reflected signals results in fault-like discontinuities in the reflections, which can lead to  
42  
43 misinterpretation (Qu et al., 2022). This seismic image is computed using full-wavefield modelling  
44  
45 based on finite difference approach, different from the convolution method used in the generation  
46  
47 of the training data, thus can contain different seismic features introduced by smearing effect,  
48  
49 multiples, converted waves, as well as further processing such as migration. However, we have  
50  
51 tried to reduce the difference caused by different seismic modelling processes. We computed  
52  
53 synthetics for the geological model shown in Figure 7b using the convolution method using 2D  
54  
55  
56  
57

1  
2  
3 Ricker wavelets with different parameters, found the 2D Ricker wavelet that can generate a seismic  
4 image similar to the one shown in Figure 7a, and used this wavelet to generate the synthetics of  
5 the training dataset.  
6  
7  
8  
9

10 Figure 7c shows the result predicted by the trained neural network. The prediction is  
11 successful in terms of the quantity of the individual layers, the thickness and geometry of the layers,  
12 and even the complex bedding architectures. In fact, the new features such as onlap and downlap  
13 are predicted. Continuity artifacts exist, particularly at places where two flint layers are too close  
14 to each other.  
15  
16  
17  
18  
19  
20  
21

### 22 **Test on real seismic data**

23  
24  
25 The acquisition and processing of seismic data can introduce some complex features that  
26 are not present in the synthetic training examples. We now test the trained convolutional neural  
27 network with real seismic data - a seismic profile acquired from the upper Maastrichtian–Danian  
28 chalk succession at the Stevns peninsula in Denmark (Kammann et al., 2019).  
29  
30  
31  
32  
33  
34

35 The seismic profile is close to a coastal cliff and a quarry with exposed chalk sections. We  
36 apply the trained neural network on the top section of the seismic profile (Figure 8a), so we can  
37 assess the quality of the prediction result by comparing to the exposed sections. It needs to be  
38 mentioned that the outcropping sections cannot be used to verify the details of the predicted layers  
39 directly, since there is a distance of around 80 m between the seismic section and the coastal cliff.  
40 However, the number of layers and the overall geometrical characteristics can be approximately  
41 inferred, thus the outcropping sections can be used to realistically verify the number and the overall  
42 geometry of the predicted layers. The succession of interest comprises 20–30m of chalk of latest  
43 Cretaceous (Maastrichtian) age and 10–20m of bryozoan limestone of Early Paleocene (Danian)  
44 age. The upper Maastrichtian part contains 10–12 flint layers with variable spacing distance  
45  
46  
47  
48  
49  
50  
51  
52  
53  
54  
55  
56  
57

1  
2  
3 (Surlyk et al., 2013), and exhibits gently wavy to almost horizontal bedding. The Danian part  
4 contains around 8–10 flint layers with variable spacing distance (Surlyk et al., 2013), and displays  
5 mound structures which are typically 50-100 m long (Surlyk et al., 2006; Figure 8b). This seismic  
6 data displays complex reflection patterns with undulations and terminations (Figure 8a). It shows  
7 weak reflectivity in the top section, and strong reflection at around 20–30 ms, which is consistent  
8 with the boundary between the Maastrichtian and Danian formations. This strong reflection can  
9 be traced throughout the section, except at an interruption at distance of 200 meters, which is most  
10 likely caused by a low fold. Please refer to Kammann et al. (2019) for details of the acquisition  
11 and processing of the data.  
12  
13  
14  
15  
16  
17  
18  
19  
20  
21  
22  
23

24 Figure 8c shows the result predicted by the trained neural network. The amplitude of the  
25 seismic data has been scaled to range between -1 and 1 before prediction. The run-time of this  
26 prediction process is in the order of seconds. Around 20 flint layers are predicted for this  
27 succession, 8–10 wavy flint layers in the Danian formation in the upper succession and 10–12  
28 gently wavy to horizontal flint layers in the Maastrichtian formation in the lower succession. These  
29 are consistent with what observed from the outcropping sections. The observed mound structures  
30 with typical length of 50–100 m are also predicted. Thus, the trained neural network is able to  
31 predict the quantity of flint layers and their geometries, even on real seismic data, which is much  
32 noisier than the synthetic training data. Similar with the first two tests, continuity artifacts mostly  
33 likely exist. Note that the 2D wavelet (Figure 2) used to generate the synthetic seismic of the  
34 training examples has not been particularly adjusted to produce smearing and other effects similar  
35 to that of the real seismic, and it is expected that a tailored wavelet can improve the performance  
36 of the trained deep learning model.  
37  
38  
39  
40  
41  
42  
43  
44  
45  
46  
47  
48  
49  
50  
51  
52  
53  
54  
55  
56  
57  
58  
59  
60

## DISCUSSION AND CONCLUSION

We have illustrated how to generate synthetic training data for supervised deep learning and investigated the capability of deep learning trained on synthetic data for predicting sub-resolution thin layers from seismic data, exemplified by an interbedded chalk-flint sequence scenario in onshore Denmark.

The result is promising as the network is able to predict a realistic number of thin layers and their overall geometries from real seismic data, despite the presence of effects such as interference and smearing, which challenge the interpretation of sub-resolution thin layers. The network can also generalize and predict more complex bedding structures not seen before. Moreover, we found that even though the neural network is trained using synthetic seismic data with a Ricker wavelet, the trained neural network can still perform a good job on the unseen real seismic data which may have different wavelet type and phase. This finding is a positive result for future application.

Continuity artifacts exist in the predicted results, this is because the flint layers are so thin that even tiny inaccuracy in predicted position can lead to discontinuity. However, the prediction result is useful in relation to overall geological characterization and for engineering purposes (e.g. construction site evaluations) in which the main concern is the number of hard flint layers present in the sequence. For other applications in which the continuity is a main focus, the following work can be conducted for improved predictions, e.g., increasing the number of pixels representing the thin layers, adjusting the wavelet used for computing the synthetics or improving the processing of the real seismic data to minimize their difference, testing different neural network architectures, hyper-parameters and loss functions. Data augmentation may also help to improve the network performance.

1  
2  
3 The synthetic training dataset is generated via stochastic geological modelling and seismic  
4 forward modelling. Over the past decades, stochastic geological modeling methods have been  
5 developed for generating multiple geological scenarios and realizations for capturing  
6 heterogeneities and uncertainties. Strategies such as utilizing information obtained from outcrop  
7 analogues have been applied for better constraining the modeling and reducing the uncertainties.  
8 We believe that these stochastic modeling methods and strategies can be readily transferred to the  
9 new deep learning regime in geoscience for generating diverse and realistic training datasets. The  
10 presented stochastic geological modeling method allows for the generation of a large number of  
11 synthetic examples and incorporation of known geological knowledge which help to generate  
12 relevant geological models. The synthetic seismic images are generated by performing a  
13 convolution operation between the 2D reflectivity models converted from the geological models  
14 and a 2D wavelet. The 2D wavelet can be adjusted to produce seismic features (e.g. smearing  
15 effects) similar to those existed in the real seismic data.  
16  
17  
18  
19  
20  
21  
22  
23  
24  
25  
26  
27  
28  
29  
30  
31  
32

33 We have generated 5000 synthetic seismic images with a dominant frequency of 150 Hz  
34 and 5000 ground truth labels, each has  $256 \times 256$  pixels and trained a U-net model, which can  
35 predict the thin flint layers from the seismic data that have been acquired from the chalk succession  
36 onshore Denmark. The thickness of the interval of interest is about 40 m and the wavelet is  
37 assumed to be constant in the selected time window. The choice of dominant frequency of wavelet  
38 for generating the synthetics is based on the dominant frequency of the real seismic data on which  
39 the prediction is to be made. Different frequencies should be used for generating the training data  
40 if predictions need to be made on seismic data with different frequencies.  
41  
42  
43  
44  
45  
46  
47  
48  
49  
50  
51

52 It is expected that the strategy and workflow presented in this paper can be transferred to  
53 solve other similar problems with new training data, and readers who are interested are more than  
54  
55  
56  
57

1  
2  
3 welcome to test the applicability of the presented training dataset in different geological settings  
4  
5 with similar bedding configurations, e.g., interbedded layers of sandstone and shale. The training  
6  
7 dataset is available at [https://github.com/GeoDQ/Interbedding\\_Dataset](https://github.com/GeoDQ/Interbedding_Dataset).  
8  
9  
10  
11  
12

### 13 ACKNOWLEDGEMENT

14  
15  
16 The research leading to these results has received funding from the Danish Hydrocarbon Research  
17  
18 and Technology Centre under the AWF-1 program. Janina Kammann is acknowledged for  
19  
20 providing the seismic data published in Kammann et al (2019).  
21  
22

### 23 REFERENCES

24  
25  
26 Anderskov, K., T. Damholt, and F. Surlyk, 2007, Late Maastrichtian chalk mounds, Stevns  
27  
28 Klint, Denmark—combined physical and biogenic structures: *Sedimentary Geology*, **200**, 57-72.  
29  
30  
31 Dramsch, J.S., 2020, 70 years of machine learning in geoscience in review: *Advances in*  
32  
33 *geophysics*, **61**, 1-55.  
34  
35  
36 Feng, R., D. Grana, and N. Balling, 2021, Uncertainty quantification in fault detection using  
37  
38 convolutional neural networks: *Geophysics*, **86**, 41-48.  
39  
40  
41 Ioffe, S., and C. Szegedy, 2015, Batch normalization: Accelerating deep network training by  
42  
43 reducing internal covariate shift, *in* International conference on machine learning, 448–456.  
44  
45  
46 Kammann, J., A. Malehmir, B. Brodicy, M. Tagliavento, L. Stemmerik, E. Nørmark, H. Lykke-  
47  
48 Andersen, and L. Nielsen, 2019, Deep onshore reflection seismic imaging of the Chalk Group strata  
49  
50 using a 45-kg accelerated weight-drop and combined recording systems with dense receiver  
51  
52 spacing: *Geophysics*, **84**, 259-268.  
53  
54  
55  
56  
57  
58  
59  
60

- 1  
2  
3 Kingma, D.P. and J. Ba, 2014, Adam: A method for stochastic optimization: arXiv, 1412.6980.  
4  
5  
6 Janson, X. and D.D. Madriz, 2012, Geomodelling of carbonate mounds using two-point and  
7  
8 multipoint statistics: Geological Society, London, Special Publications, **370**, 229-246.  
9  
10  
11 Li, S., C. Yang, H. Sun, and H. Zhang, 2019, Seismic fault detection using an encoder–decoder  
12  
13 convolutional neural network with a small training set: Journal of Geophysics and Engineering,  
14  
15 **16**, 175-189.  
16  
17  
18 Merrifield, T.P., D.P. Griffith, S.A. Zamanian, S. Gesbert, S. Sen, J. De La Torre Guzman, R.D.  
19  
20 Potter, and H. Kuehl, 2022, Synthetic Seismic Data for Training Deep Learning Networks:  
21  
22 Interpretation, **10**, 1-52.  
23  
24  
25  
26 Nair, V., and G.E. Hinton, 2010, Rectified linear units improve restricted Boltzmann machines, *in*  
27  
28 Proceedings of the 27th international conference on machine learning (ICML-10), 807–814.  
29  
30  
31 Nielsen, L., L.O. Boldreel, T.M. Hansen, H. Lykke-Andersen, L. Stemmerik, F. Surlyk, and H.  
32  
33 Thybo, 2011, Integrated seismic analysis of the Chalk Group in eastern Denmark—implications  
34  
35 for estimates of maximum palaeo-burial in southwest Scandinavia: Tectonophysics, **511**, 14-26.  
36  
37  
38 Phan, S.D.T., 2021, Machine learning algorithms for solving some seismic inversion challenges:  
39  
40 Doctoral dissertation, The University of Texas at Austin.  
41  
42  
43 Qu, D., K. Anderskov, L. Stemmerik, and L. Nielsen, 2022, Seismic interpretation pitfalls  
44  
45 caused by interference effects, exemplified by seismic modeling of outcropping chalk  
46  
47 successions: Interpretation, accepted.  
48  
49  
50  
51 Rahman, M.A., and Y. Wang, 2016, Optimizing intersection-over-union in deep neural networks  
52  
53 for image segmentation, *in* International symposium on visual computing: Springer, Cham, 234-  
54  
55 244.  
56  
57

1  
2  
3 Ronneberger, O., P. Fischer, and T. Brox, 2015, U-net: Convolutional networks for biomedical  
4 image segmentation, *in* International Conference on Medical image computing and computer-  
5 assisted intervention: Springer, Cham, 234-241.  
6  
7

8  
9  
10 Surlyk, F., T. Damholt, and M. Bjerager, 2006, Stevns Klint, Denmark: uppermost Maastrichtian  
11 chalk, Cretaceous-Tertiary boundary, and lower Danian bryozoan mound complex: Bulletin of the  
12 Geological Society of Denmark, **54**, 1-48.  
13  
14  
15

16  
17  
18 Surlyk, F., S. L. Rasmussen, M. Boussaha, P. Schiøler, N. H. Schovsbo, E. Sheldon, L. Stemmerik,  
19 and N. Thibault, 2013, Upper Campanian-Maastrichtian holostratigraphy of the eastern Danish  
20 Basin: Cretaceous Research, **46**, 232-256.  
21  
22  
23

24  
25 Tarantola, A., 2005, Inverse problem theory and methods for model parameter estimation: Society  
26 for Industrial and Applied Mathematics.  
27  
28

29  
30 van Beers, F., A. Lindström, E. Okafor, and M.A. Wiering, 2019, Deep Neural Networks with  
31 Intersection over Union Loss for Binary Image Segmentation, *in* ICPRAM, 438-445.  
32  
33

34  
35 Wang, Z., T. Chen, X. Hu, L. Wang, and Y. Yin, 2022, A Multi-Point Geostatistical Seismic  
36 Inversion Method Based on Local Probability Updating of Lithofacies. *Energies*, **15**, 299.  
37  
38

39  
40 Wu, X., L. Liang, Y. Shi, and S. Fomel, 2019, FaultSeg3D: Using synthetic data sets to train an  
41 end-to-end convolutional neural network for 3D seismic fault segmentation: *Geophysics*, **84**, 35-  
42 45.  
43  
44  
45

46  
47  
48 Yuan, H., M. C. Looms, and L. Nielsen, 2021, Rock physics characterization of chalk by  
49 combining acoustic and electromagnetic properties: *Geophysics*, **87**, 1-65.  
50  
51  
52

## LIST OF FIGURES

**Figure 1.** Example synthetic data. (a, b) Two geological sections with different number of layers and varying layer geometry; flint layers in yellow and chalk layers in dark blue; (c, d) Corresponding seismic images.

**Figure 2.** 2D Ricker wavelet matrix with size of  $501 \times 501$ ; sampling interval is 0.07 ms in time and 0.1 m in space. The 2D wavelet with the 'hyperbolic' shape and the decreasing amplitude away from the center simulates an imperfectly migrated (in this case under-migrated) response from a point scatterer, which is common in real seismic data.

**Figure 3.** Illustration of patches of seismic images (left) and ground truth geological images (right) used as training data

**Figure 4.** U-net architecture used in this paper

**Figure 5.** Training and validation loss

**Figure 6.** (a) Seismic image with normalized amplitude between -1 and 1; (b) Ground truth label; (c) Predicted flint and chalk layers; the red circles highlight some of the continuity artefacts.

**Figure 7.** (a) Seismic image with normalized amplitude between -1 and 1, positive in red and negative in blue; (b) Geological section corresponding to the seismic section; the blue circles highlight some complex bedding features not present in the training examples; (c) Predicted flint and chalk layers; the complex bedding features are highlighted with the blue circles.

**Figure 8.** (a) Seismic data collected from the Danian and Upper Maastrichtian chalk succession at the Stevns peninsula in Denmark (Kammann et al., 2019); (b) Stitched image of outcropping chalk succession not far from the seismic profile; the upper section is from the coastal cliffs, the lower section is from a quarry close the cliff; (c) Predicted flint and chalk layers

1  
2  
3  
4  
5  
6  
7  
8  
9  
10  
11  
12  
13  
14  
15  
16  
17  
18  
19  
20  
21  
22  
23  
24  
25  
26  
27  
28  
29  
30  
31  
32  
33  
34  
35  
36  
37  
38  
39  
40  
41  
42  
43  
44  
45  
46  
47  
48  
49  
50  
51  
52  
53  
54  
55  
56  
57  
58  
59  
60

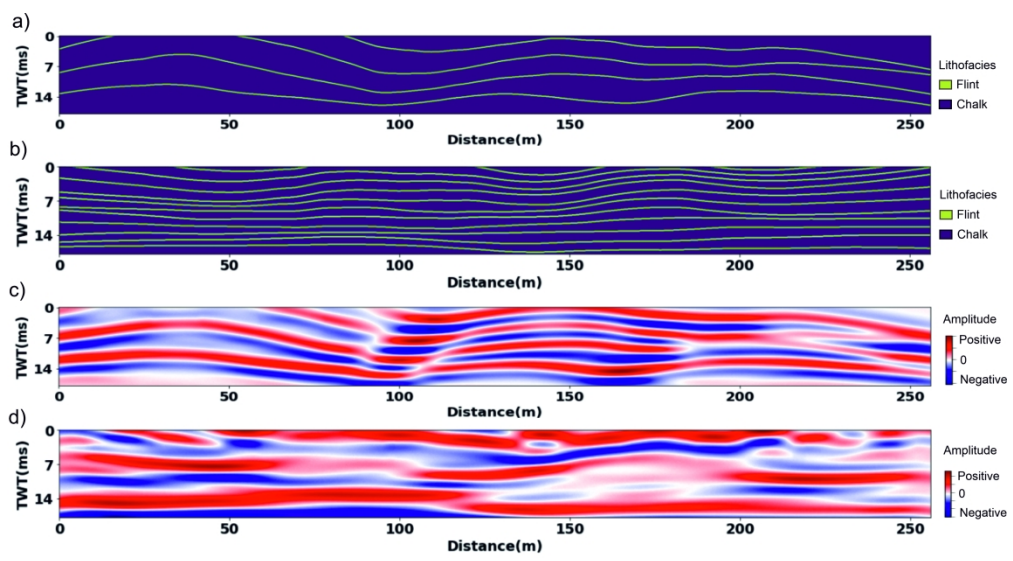


Figure 1. Example synthetic data. (a, b) Two geological sections with different number of layers and varying layer geometry; flint layers in yellow and chalk layers in dark blue; (c, d) Corresponding seismic images.

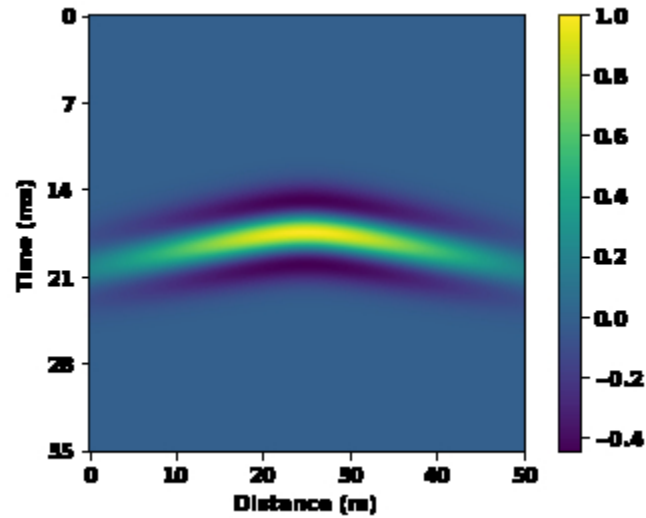


Figure 2. 2D Ricker wavelet matrix with size of  $501 \times 501$ ; sampling interval is 0.07 ms in time and 0.1 m in space. The 2D wavelet with the 'hyperbolic' shape and the decreasing amplitude away from the center simulates an imperfectly migrated (in this case under-migrated) response from a point scatterer, which is common in real seismic data.

296x241mm (28 x 28 DPI)

1  
2  
3  
4  
5  
6  
7  
8  
9  
10  
11  
12  
13  
14  
15  
16  
17  
18  
19  
20  
21  
22  
23  
24  
25  
26  
27  
28  
29  
30  
31  
32  
33  
34  
35  
36  
37  
38  
39  
40  
41  
42  
43  
44  
45  
46  
47  
48  
49  
50  
51  
52  
53  
54  
55  
56  
57  
58  
59  
60

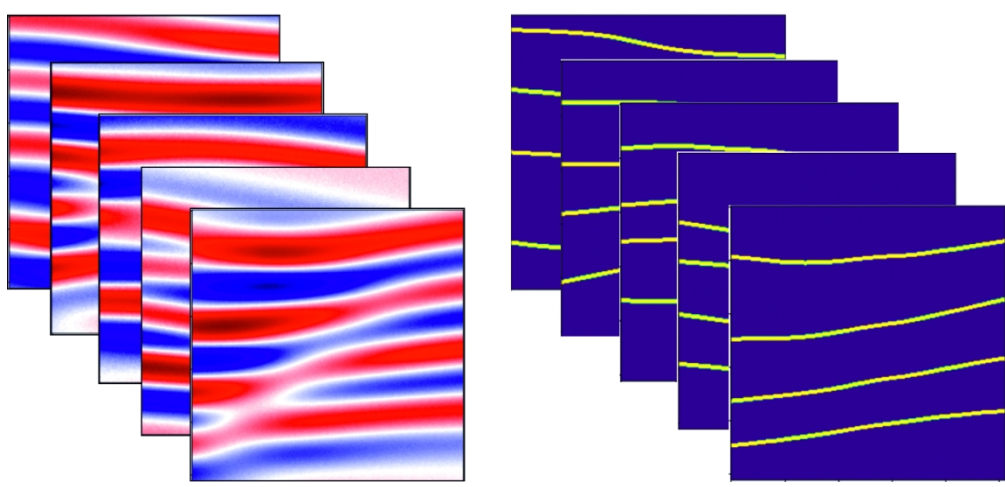


Figure 3. Illustration of patches of seismic images (left) and ground truth geological images (right) used as training data

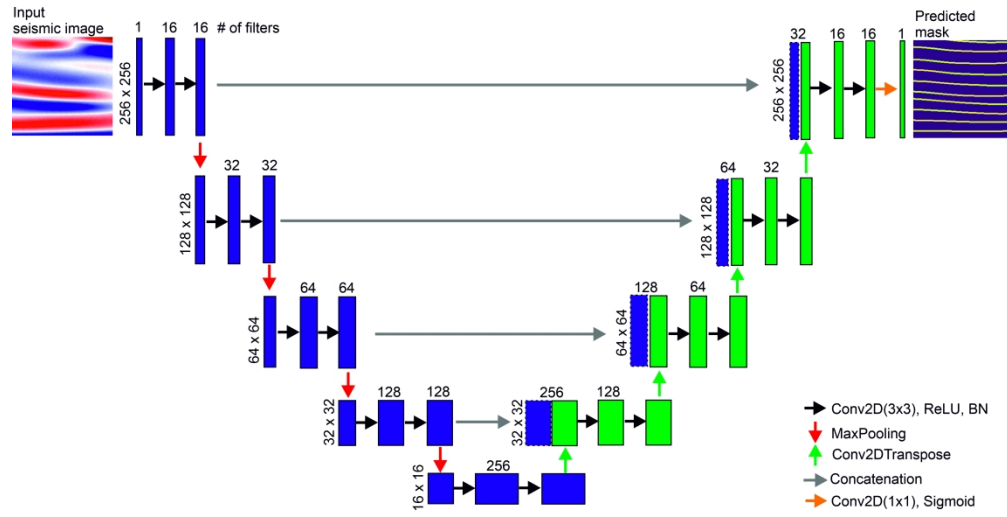


Figure 4. U-net architecture used in this paper

1  
2  
3  
4  
5  
6  
7  
8  
9  
10  
11  
12  
13  
14  
15  
16  
17  
18  
19  
20  
21  
22  
23  
24  
25  
26  
27  
28  
29  
30  
31  
32  
33  
34  
35  
36  
37  
38  
39  
40  
41  
42  
43  
44  
45  
46  
47  
48  
49  
50  
51  
52  
53  
54  
55  
56  
57  
58  
59  
60

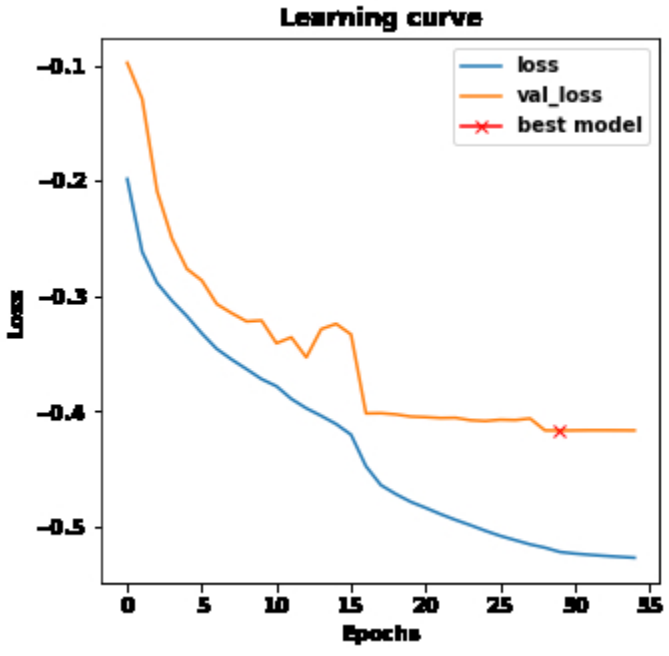


Figure 5. Training and validation loss  
310x302mm (28 x 28 DPI)

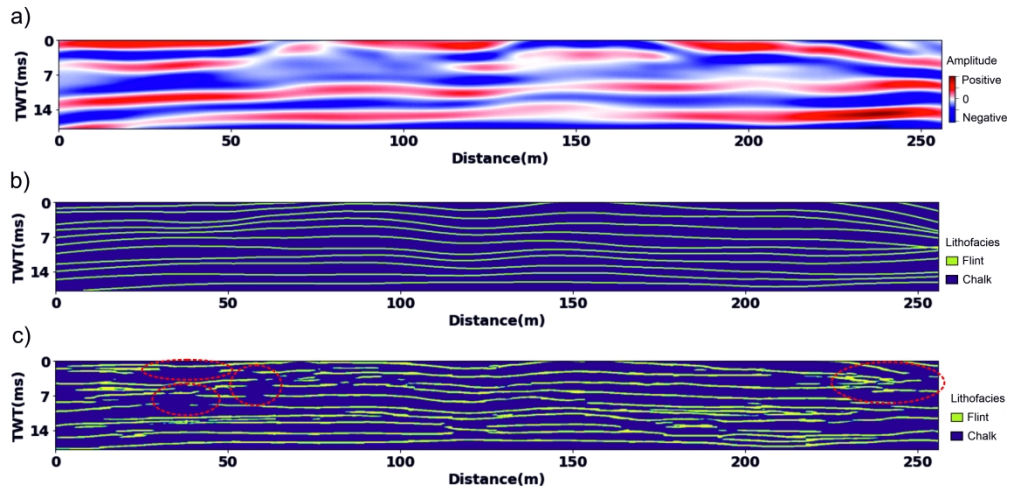


Figure 6. (a) Seismic image with normalized amplitude between -1 and 1; (b) Ground truth label; (c) Predicted flint and chalk layers; the red circles highlight some of the continuity artefacts.

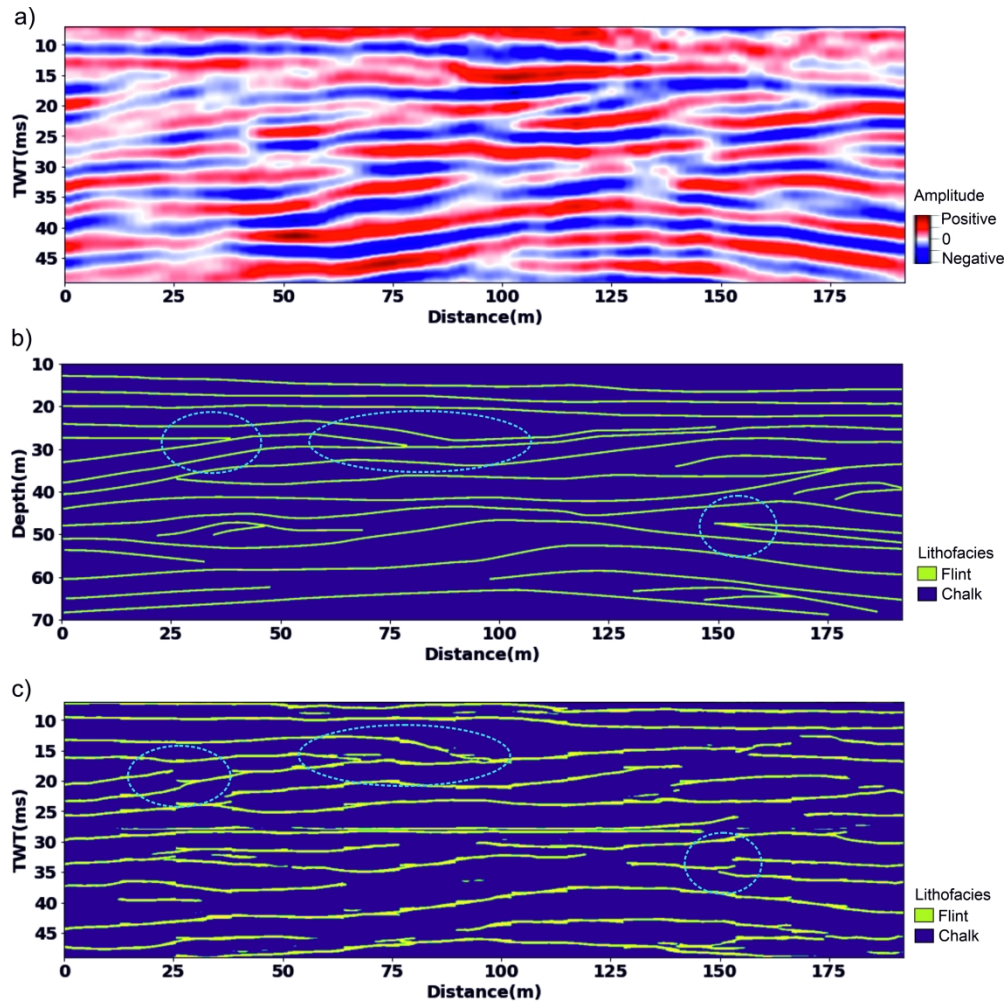


Figure 7. (a) Seismic image with normalized amplitude between -1 and 1, positive in red and negative in blue; (b) Geological section corresponding to the seismic section; the blue circles highlight some complex bedding features not present in the training examples; (c) Predicted flint and chalk layers; the complex bedding features are highlighted with the blue circles.

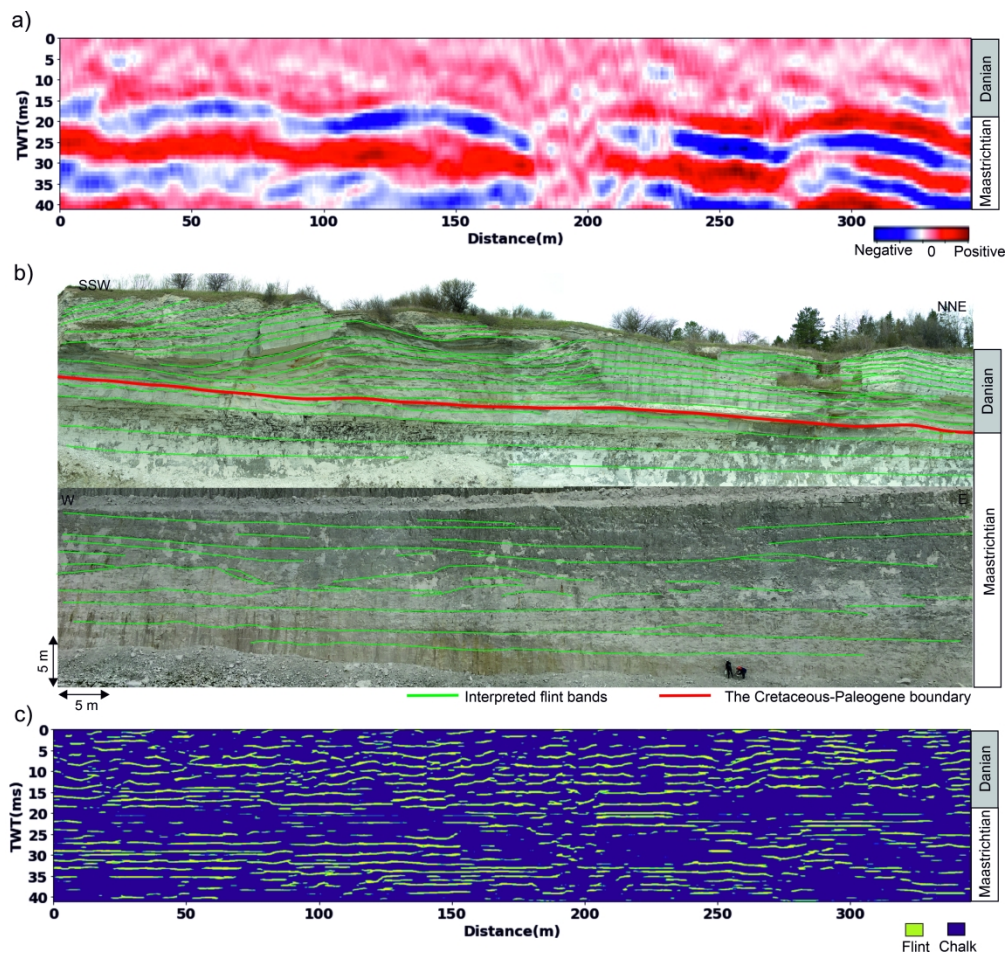


Figure 8. (a) Seismic data collected from the Danian and Upper Maastrichtian chalk succession at the Stevns peninsula in Denmark (Kammann et al., 2019); (b) Stitched image of outcropping chalk succession not far from the seismic profile; the upper section is from the coastal cliffs, the lower section is from a quarry close the cliff; (c) Predicted flint and chalk layers